ACS APPLIED MATERIALS & INTERFACES

Research Article

www.acsami.org

Transfer Printed Silver Nanowire Transparent Conductors for PbS–ZnO Heterojunction Quantum Dot Solar Cells

Natasha E. Hjerrild,[†] Darren C. J. Neo, Assia Kasdi, Hazel E. Assender, Jamie H. Warner, and Andrew A. R. Watt*

Department of Materials, University of Oxford, Parks Road, Oxford, OX1 3PH, U.K.

Supporting Information

ABSTRACT: Transfer-printed silver nanowire transparent conducting electrodes are demonstrated in lead sulfide–zinc oxide quantum dot solar cells. Advantages of using this transparent conductor technology are increased junction surface energy, solution processing, and the potential cost reduction of low temperature processing. Joule heating, device aging, and film thickness effects are investigated to understand shunt pathways created by nanowires protruding perpendicular to the film. A V_{oc} of 0.39 ± 0.07 V, J_{sc} of 16.2 ± 0.2 mA/cm^2, and power conversion efficiencies of 2.8 ± 0.4% are presented.

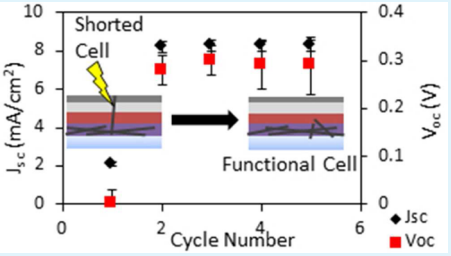

KEYWORDS: *solution processed solar cells, nanoparticles, ITO-free, transparent electrodes, photovoltaics, surface roughness*

1. INTRODUCTION

Solution-processed solar cells have the potential to become an inexpensive energy technology to rival silicon solar cells.[1−3] Semiconductor colloidal quantum dot (CQD) photovoltaic (PV) devices have shown a steady increase in efficiency over the past decade increasing from 4% to over 8% in the space of four years.[4−6] The low temperatures required for CQD synthesis and the potential for high-throughput, roll-to-roll deposition of QD ink make them a very attractive technology.[7] To date, most CQD PV devices have used either metal conductive oxide or graphene films as the transparent back contact.[8,9] In this paper we replace these with solution processed, transfer-printed silver nanowire transparent thin film contacts and investigate the influence of underlying film morphology on device performance.

Thin silver (Ag) films are of interest due to the high electrical conductivity of silver and the high demand, limited supply, and consequentially high price of indium used in the industry standard transparent conductor, indium doped tin oxide (ITO).[10,11] Sputtered thin Ag films (<10 nm), have been used as an alternative transparent conductor (TC) to ITO in organic solar cells. These devices produced equivalent conversion efficiencies to those fabricated with ITO due to the similar electronic and optical properties of the two transparent conductors.[12] However, sputter coating is a wasteful deposition process and necessitates a high vacuum environment, resulting in low-throughput device fabrication, and ultimately higher device cost.[13]

Silver nanowires (Ag NWs) with aspect ratios >100 have been shown to form low density, highly interconnected networks with low sheet resistances and good optical transparency.[14] Optimizing NW deposition techniques, which control the NW density and relative arrangement on a substrate, is key to forming high-quality transparent conducting NW films.[14,15] Some groups have fabricated organic solar cells using Ag NW TCs to replace ITO, yielding a peak efficiency of 3.8%.[1,3] One potential benefit of the Ag NW films is that they can provide a higher heterojunction area thus increasing the potential for charge collection. We suggest this because NW films are inherently three-dimensional thus increasing the interfacial area of subsequent layers; this has previously been identified as beneficial to device performance.[16]

2. EXPERIMENTAL METHODS

All nanocrystal solutions (Ag NWs, ZnO, and PbS QDs) were synthesized using previously published methods and are described in the Supporting Information.[7,17,18] From scanning electron microscopy analysis we find that the as deposited NWs were on average 13 ± 0.8 μm in length. PbS CQDs used here had an average band gap of 1.27 eV (σ = 85 meV, fwhm = 121 meV).

For fabrication of each Ag NW transparent conductor (TC), 600 μL of a low concentration Ag NW–methanol solution (0.016 wt %) was deposited on glass by a vacuum filter printing technique using Omnipore hydrophilic PTFE filters with 10 μm diameter pores. Deposited NW films were heated at 200 °C for 2 h before applying silver paint contacts at the film edge for solar simulator testing. This deposition process produced Ag NW films with an average thickness of 160 nm as measured by a Veeco DekTak 6 M Stylus Profilometer and typical sheet resistance of 10 ± 2 Ω/□ as measured by four-point probe. Transmittances were measured using an integrating sphere-equipped absorption spectrometer and are presented in the Supporting Information (Figure S1). Images of surface morphology were obtained using a MicroXAM Optical Profiler.

The solar cell geometry and band structure are shown in Figure 1a and b, respectively. Figure 1b shows that a type-II heterojunction forms between the n-type ZnO and p-type PbS. After Ag NW TC

Received: August 21, 2014
Accepted: March 13, 2015
Published: March 13, 2015

DOI: 10.1021/am505646d
ACS Appl. Mater. Interfaces 2015, 7, 6417−6421

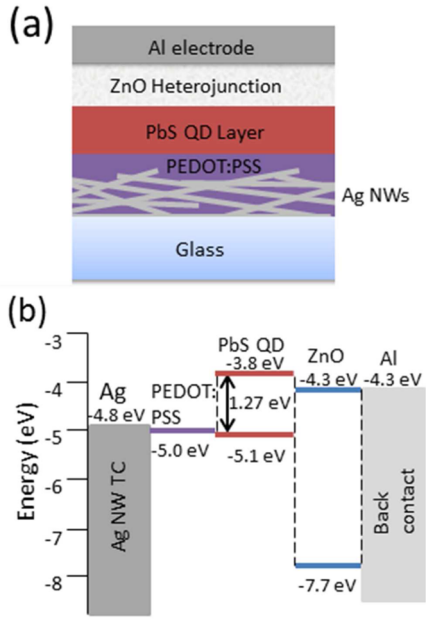

Figure 1. (a) Physical structure (not to scale) and (b) energy diagram for devices.

fabrication, PEDOT:PSS was deposited by a 60 s spin coat process at 5000 rpm and then dried at 110 °C for 30 min. The PbS QD film consisted of 5 independently deposited layers, each consisting of 1 drop of QD solution followed by 2 drops of 1 vol % 1,2-ethanedithiol in methanol, 5 drops of methanol, 5 drops of toluene, and 5 more drops of methanol while spin coating at 2000 rpm. Devices were plasma treated for 15 s in an H_2/N_2 environment before ZnO solution was deposited by spin coating at 1000 rpm. A second layer of ZnO was then spun coated at 2000 rpm for further NW encapsulation. Finally, a 100 nm aluminum top contact was deposited by evaporation. The Ag NW were replaced with ITO to act as a control device.

Device power conversion efficiency (PCE) was evaluated by illuminating devices using a xenon lamp fitted with a filter to simulate AM1.5 solar irradiation and measured using a Keithley 2400 Source Measurment Unit, the power density of the light source was calibrated using an ABET technologies 15151 Calibrated Silicon Reference Cell. For external quantum efficiency (EQE) measurements illumination was provided by a halogen lamp and Oriel Conerstone 130 monochromator. Light intensity at different wavelengths was calibrated using a Newport 818 UV enhanced silicon photodetector and a Newport 918 IR germanium photodetector. The current signal was measured with a Keithley 6845 picoammeter. All device performance testing took place under N_2 flow to reduce PbS QD degradation Three identically fabricated devices were fabricated for each NW thickness means and errors were calculated according to the variance of five measurements on each device.

3. RESULTS AND DISCUSSION

The morphology of the thin film layers as they are built up is shown in Figure 2. It can be seen in parts a–c that the building up of the PEDOT:PSS, PbS, and ZnO on the nanowires creates a very rough surface which penetrates right through to the PbS layer. While the corresponding ITO layers parts d–f are much smoother, there are obvious cracks which arise from the replacement of the long chain oleic acid ligands with the much shorter ethanedithiol which causes stress to build up in the films which needs to be relaxed by tessellations.

Upon device fabrication we found that a large percentage of the devices fabricated were prone to short circuiting, which we believed to be caused by NW penetration through the cell to the aluminum top contact. We hypothesized that these short circuits could be destroyed by passing sufficient current to cause joule heating of the nanowire, as this has been shown to break nanowires and create nonconductive pathways.[19] To test this, devices were cycled between −0.5 and 1.0 V under illumination in an attempt to destroy NW–Al contact short pathways.

As Figure 3 shows, a drastic change in J–V behavior occurs over the course of five −0.5 V to 1.0 V voltage sweeps in both forward and reverse bias of a device under solar illumination. The solar cell progressed from a completely short-circuiting device with R_{shunt} value of 10 Ω cm^2 upon the first voltage sweep to a rectifying device with an increase in R_{shunt} by almost 2 orders of magnitude upon the second voltage sweep. Subsequent voltage sweeps show no sign of significant short-circuiting and the device parameters typically plateau to a stable

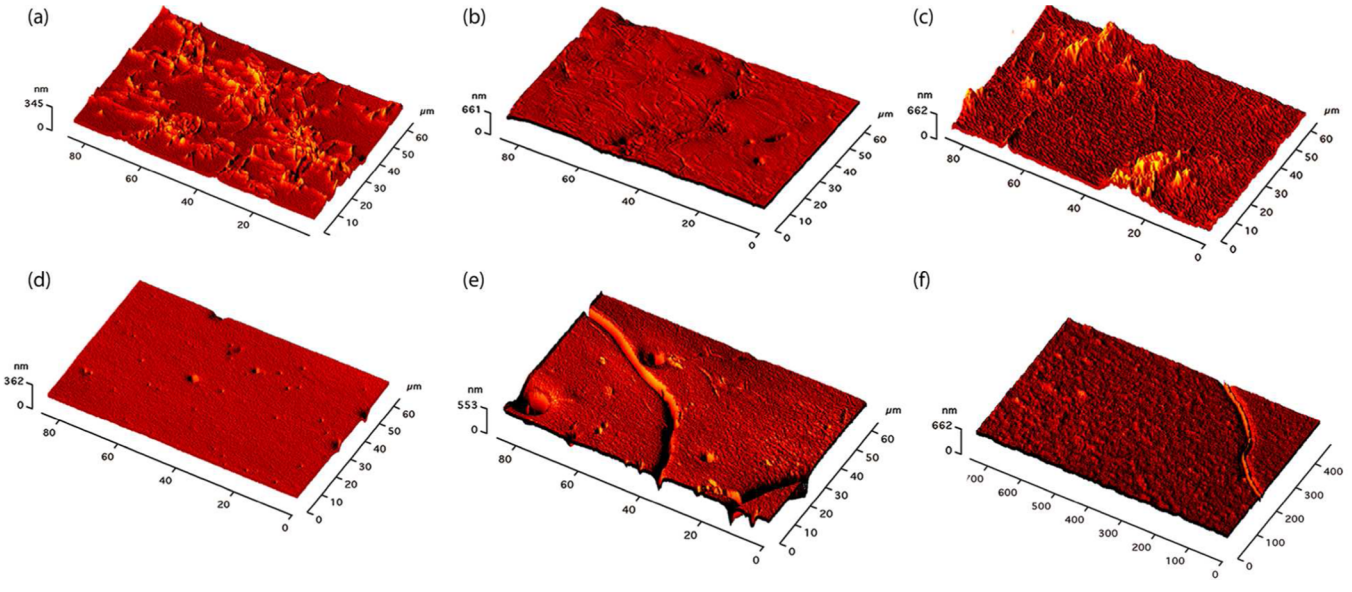

Figure 2. MicroXam surface profile images of (a) glass–Ag NW–PEDOT:PSS, (b) glass–Ag NW–PEDOT:PSS-PbS, (c) glass–Ag NW–PEDOT:PSS–PbS–ZnO, (d) glass–ITO–PEDOT:PSS, (e) glass–ITO–PEDOT:PSS–PbS, (f) glass–ITO–PEDOT:PSS–PbS–ZnO.

DOI: 10.1021/am505646d
ACS Appl. Mater. Interfaces 2015, 7, 6417–6421

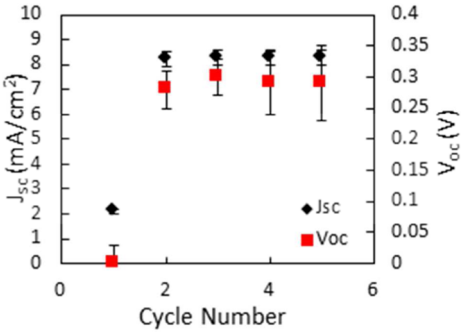

Figure 3. Plot of improved device performance with multiple applied voltage cycles. The device performance improved substantially from the first −0.5 to 1.0 V voltage cycle to the second −0.5 to 1.0 V voltage cycle, implying breakup of NWs in contact with the Al electrode. After nanowire break up, J_{sc} and V_{oc} values stabilized.

V_{oc} of 0.29 ± 0.05 V, J_{sc} of 8.3 ± 0.3 mA/cm^2, and PCE of 1.0% ± 0.2%, respectively. Control devices made at the same time using the same batch of ZnO and PbS CQD inks using ITO had V_{oc} of 0.38 ± 0.06 V, J_{sc} of 10.75 ± 0.7 mA/cm^2, and PCE of 1.5% ± 0.4%. Therefore, compared to the ITO control devices the nanowire devices performed reasonably well. Errors were calculated using the variance in J_{sc} and V_{oc} measurements for forward and reverse bias application to the device for at least five devices.

The Ag NW−PbS QD solar cells typically produced a leakage current density (J_o) of 1.0 ± 0.3 μA/cm^2, which is a full order of magnitude greater than that of devices fabricated using an ITO TC. Because device V_{oc} increases logarithmically with the inverse of J_o, a large leakage current yields a low V_{oc} and consequentially poor cell efficiency.[20] There are two proposed causes for the J_o increase and V_{oc} reduction: (1) low-density Ag NW penetration through the photoactive layers and (2) disruption of a uniform PbS CQD film caused by the comparatively high roughness Ag NW substrate.

Some devices that performed poorly upon initial testing also improved dramatically with aging in an N_2 environment. This is shown in Figure 4, V_{oc} rises from 0.21 ± 0.07 to 0.39 ± 0.07 V of a device tested immediately after aluminum contact deposition and then after an 18 h aging process. During this aging process, the cells were left in a dark N_2 environment, and no bias was applied. We attribute reduced shunt pathways, indicated by the increase of R_{shunt} from 600 ± 200 to 1100 ± 200 Ω cm^2 over this aging period, to the rise in V_{oc} and

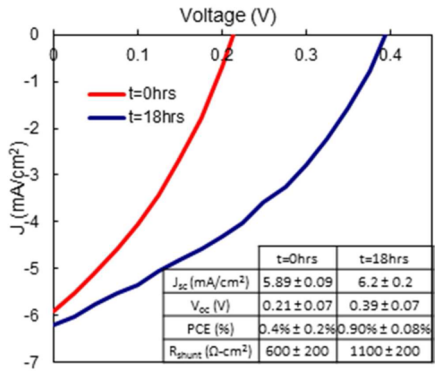

Figure 4. Device J−V plot and performance metrics before (t = 0 h, red) and after (t = 18 h, blue) aging in N_2 environment.

consequential jump in PCE from 0.4% ± 0.2% to 0.90% ± 0.08%.

Two mechanisms have been proposed to explain the observed short-circuit passivation by device aging. First, the low temperatures (<175 °C), supplied by joule heating of Ag NWs,[19] may cause metallic clusters and defects to develop in the ZnO film. At these sites of Ag NW penetration in the ZnO film, the ZnO would become semi-insulative, as has been reported in intentionally Ag-doped ZnO films.[21] Alternatively, an Ag_xO_y shell may form when O_2 is desorbed from the ZnO film during both UV-photodoping and heat treatment caused by joule heating.[22] Because the resistivity of silver oxides is over 10 orders of magnitude greater than that of Ag,[23] shunt pathways could then be reduced by the formation of a Ag_xO_y shell around the nanowire which results in improved device performance. After functional cells could be consistently fabricated with aging improvement, the Ag NW density was altered in an attempt to further increase device performance.[14]

Ag NW film density was varied by depositing Ag NW solution in various volumes to test the effects of NW film conductivity and morphology on device performance. The dilute Ag NW−methanol solution was deposited in volumes of 200, 400, 600, 800, and 1000 μL. These volumes relate to average Ag NW film thicknesses of 130, 140, 160, 220, and 260 nm, respectively, as measured by a Veeco DekTak 6 M Stylus Profilometer. Images of the resulting Ag NW films can be found in the Supporting Information (Figure S2).

Cell performance using these varying Ag NW densities after 18 h of aging in an N_2 environment is shown in Figure 5. Figure 5a shows that thicker Ag NW films result in lower R_{series}, which follows the trend of reduced R_{sheet} with greater Ag NW film thickness noted in Figure 5b. Although low R_{series} devices typically result in high J_{sc} devices, denser Ag NW films result in higher roughness films, shown in Figure 5b. It is proposed that higher density NW films lead to increased disruption of later-deposited films, resulting in greater short-circuiting. Furthermore, higher density NW films result in greater maximum peak heights caused by substantial Ag NW overlap and deposited NWs penetrating out of plane, which provide additional paths for short-circuiting. Greater shunt pathways with increased NW density correlates to reduced R_{shunt} and V_{oc} values, as shown in Figure 5a and c, respectively. Figure 4d indicates that this V_{oc}−J_{sc} trade-off results in an optimal PCE for Ag NW TCs with an average thickness of 160 nm and a completely short-circuited device for Ag NW TCs > 260 nm thick.

The external quantum efficiency (EQE) for a device fabricated using a 160 nm thick Ag NW TC is compared to a PbS QD cell fabricated using exactly the same method on ITO and is shown in Figure 6a. The performance of the nanowire device is much poorer toward the UV, this is most likely to be due to the formation of dead-zone due to a combination of thin film optical effects and poor extraction of charges toward the front of the cell.[24] The slight red-shift of the ITO based devices excitonic peak is unusual but could be due to increased oxidation of the PbS in the Ag NW device resulting in a decrease of the QD size. As can be seen in Figure 6b the transmission characteristics of the ITO device are far superior, which explains the overall increase in EQE.

Implementing a combination of joule heating, device aging under N_2 conditions, and optimal Ag NW film thickness, a champion cell with an efficiency of 2.8 ± 0.4% was achieved. This is a promising beginning to Ag NW−PbS CQD solar cells, since this early champion cell is not far from the efficiencies of

DOI: 10.1021/am505646d
ACS Appl. Mater. Interfaces 2015, 7, 6417−6421

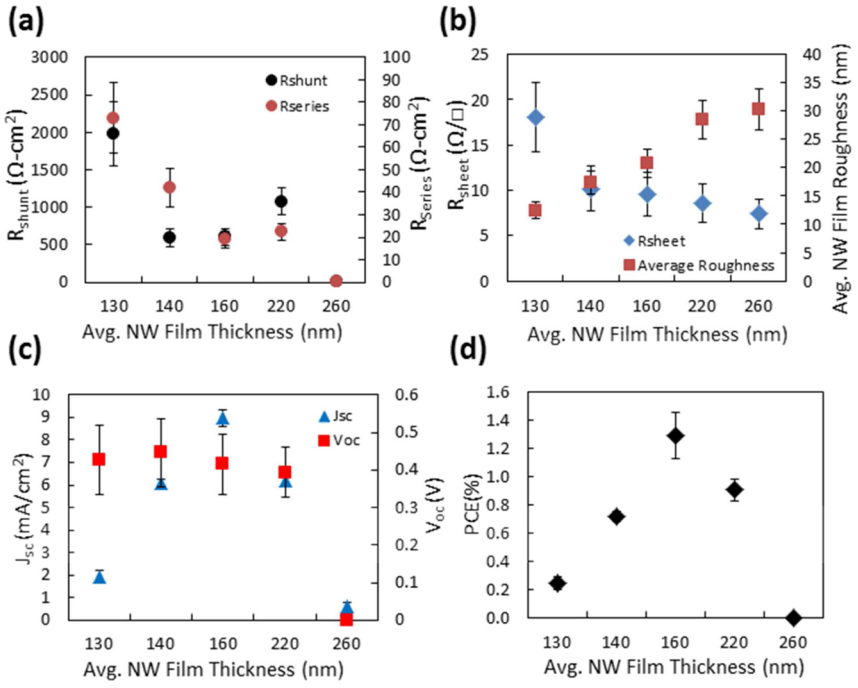

Figure 5. (a) R_{series} and R_{shunt}, (b) R_{sheet} and average Ag NW roughness, (c) J_{sc} and V_{oc}, (d) and PCE values for devices of varying Ag NW thickness.

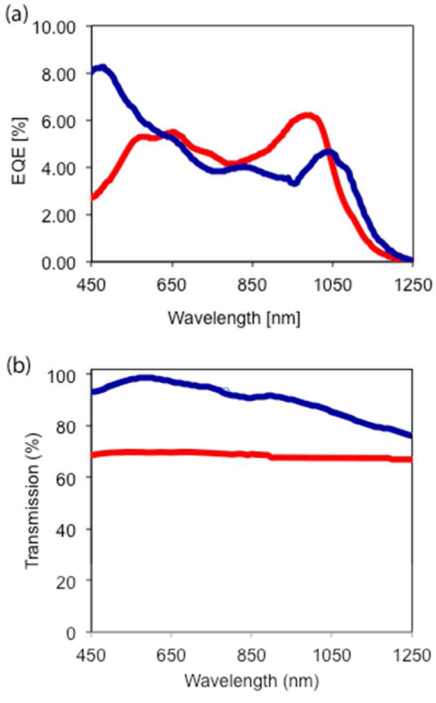

Figure 6. Wavelength dependence of (a) EQE for PbS QD devices fabricated with ITO (blue) and Ag NW TC substrates (red) and (b) transmission spectra of ITO (blue) and Ag NW (red).

similar polymer–Ag NW solar cells, which have been recently made.[1,3]

4. CONCLUSION

In conclusion, inorganic solar cells have been produced with a solution-processed silver nanowire (Ag NW) transparent conductor and lead sulfide quantum dot photoactive layers. Short-circuiting due to NW penetration of the cell and high leakage currents proved to be the greatest source of cell degradation. These detrimental effects were remediated to some extent by NW breakup caused by joule heating, slight device aging, and alteration of Ag NW film thickness, yielding a champion cell efficiency of 2.8 ± 0.4%. Further device efficiency improvement and better reproducibility is expected by reducing Ag NW-PEDOT:PSS film roughness and better encapsulation of Ag NWs penetrating through photoactive layers.

■ ASSOCIATED CONTENT

Supporting Information

Synthesis methods for silver nanowires, zinc oxide solution, and lead sulfide quantum dots. Scanning electron microscopy images of silver nanowire films of variable density. This material is available free of charge via the Internet at http://pubs.acs.org.

■ AUTHOR INFORMATION

Corresponding Author

*Electronic mail: andrew.watt@materials.ox.ac.uk.

Present Address

†N.E.H.: School of Photovoltaic and Renewable Energy Engineering, University of New South Wales, Kensington, NSW 2052, Australia.

Author Contributions

The manuscript was written through contributions of all authors. All authors have given approval to the final version of the manuscript.

Funding

We acknowledge funding from EPSRC grants EP/K032518/1 (Characterization of Nanomaterials for Energy), EP/J009857/1 (Rational design of solid-state semiconductor-sensitized solar cells: from materials modeling to device fabrication), and EP/F048009/1.

Notes

The authors declare no competing financial interest.

DOI: 10.1021/am505646d
ACS Appl. Mater. Interfaces 2015, 7, 6417–6421

ABBREVIATIONS

Ag NW = silver nanowire
CQD = colloidal quantum dot
ITO = indium tin oxide
J_{sc} = short circuit current
PbS QD = lead sulfide quantum dot
PEDOT:PSS = poly(3,4-ethylenedioxythiophene)−poly-(styrenesulfonate)
PV = photovoltaic
R_{series} = series resistance
R_{shunt} = shunt resistance
TC = transparent conductor
V_{oc} = open-circuit voltage

REFERENCES

(1) Morgenstern, F. S. F.; Kabra, D.; Massip, S.; Brenner, T. J. K.; Lyons, P. E.; Coleman, J. N.; Friend, R. H. Ag-Nanowire Films Coated with ZnO Nanoparticles as a Transparent Electrode for Solar Cells. *Appl. Phys. Lett.* **2011**, *99*, 183307.
(2) Hardin, B. E.; Gaynor, W.; Ding, I.-K.; Rim, S.-B.; Peumans, P.; McGehee, M. D. Laminating Solution-Processed Silver Nanowire Mesh Electrodes onto Solid-State Dye-Sensitized Solar Cells. *Org. Electron.* **2011**, *12*, 875−879.
(3) Ajuria, J.; Ugarte, I.; Cambarau, W.; Etxebarria, I.; Tena-Zaera, R.; Pacios, R. Insights on the Working Principles of Flexible and Efficient ITO-Free Organic Solar Cells Based on Solution Processed Ag Nanowire Electrodes. *Sol. Energy Mater. Sol. Cells* **2012**, *102*, 148−152.
(4) Lee, J.-W.; Son, D.-Y.; Ahn, T. K.; Shin, H.-W.; Kim, I. Y.; Hwang, S.-J.; Ko, M. J.; Sul, S.; Han, H.; Park, N.-G. Quantum-Dot-Sensitized Solar Cell with Unprecedentedly High Photocurrent. *Sci. Rep.* **2013**, *3*, 1−8.
(5) Kramer, I. J.; Sargent, E. H. Colloidal Quantum Dot Photovoltaics: A Path Forward. *ACS Nano* **2011**, *5*, 8506−8514.
(6) Chuang, C. M.; Brown, P. R.; Bulović, V.; Bawendi, M. G. Improved Performance and Stability in Quantum Dot Solar Cells through Band Alignment Engineering. *Nat. Mater.* **2014**, *13*, 796−801.
(7) Hines, M. A.; Scholes, G. D. Colloidal PbS Nanocrystals with Size-Tunable Near-Infrared Emission: Observation of Post-Synthesis Self-Narrowing of the Particle Size Distribution. *Adv. Mater.* **2003**, *15*, 1844−1849.
(8) Choi, J. J.; Lim, Y.; Santiago-berrios, M. E. B.; Oh, M.; Hyun, B.; Sun, L.; Bartnik, A. C.; Goedhart, A.; Malliaras, G. G.; Abrun, D.; Wise, F. W.; Hanrath, T. PbSe Nanocrystal Excitonic Solar Cells. *Nano Lett.* **2009**, *9*, 3749−3755.
(9) Park, H.; Chang, S.; Jean, J.; Cheng, J. J.; Araujo, P. T.; Wang, M.; Bawendi, M. G.; Dresselhaus, M. S.; Bulovic, V.; Kong, J.; Gradečak, S. Graphene Cathode-Based ZnO Nanowire Hybrid Solar Cells. *Nano Lett.* **2013**, *13*, 233−239.
(10) Hecht, D. S.; Hu, L.; Irvin, G. Emerging Transparent Electrodes Based on Thin Films of Carbon Nanotubes, Graphene, and Metallic Nanostructures. *Adv. Mater.* **2011**, *23*, 1482−1513.
(11) Kapilevich, I. Indium Shortage Implications for the PV Market: Technology and Market Considerations for Maintaining Growth. *34th IEEE Photovoltaic Specialists Conference*; Philadelphia, June 7−12, 2009; pp 2055−2060.
(12) O'Connor, B.; Haughn, C.; An, K.-H.; Pipe, K. P.; Shtein, M. Transparent and Conductive Electrodes Based on Unpatterned, Thin Metal Films. *Appl. Phys. Lett.* **2008**, *93*, 223304.
(13) Hecht, D. S.; Kaner, R. B. Solution-Processed Transparent Electrodes. *MRS Bull.* **2011**, *36*, 749−755.
(14) Madaria, A. R.; Kumar, A.; Zhou, C. Large Scale, Highly Conductive and Patterned Transparent Films of Silver Nanowires on Arbitrary Substrates and Their Application in Touch Screens. *Nanotechnology* **2011**, *22*, 245201.
(15) Scardaci, V.; Coull, R.; Lyons, P. E.; Rickard, D.; Coleman, J. N. Spray Deposition of Highly Transparent, Low-Resistance Networks of Silver Nanowires over Large Areas. *Small* **2011**, *7*, 2621−2628.
(16) Barkhouse, D. A. R.; Debnath, R.; Kramer, I. J.; Zhitomirsky, D.; Pattantyus-Abraham, A. G.; Levina, L.; Etgar, L.; Grätzel, M.; Sargent, E. H. Depleted Bulk Heterojunction Colloidal Quantum Dot Photovoltaics. *Adv. Mater.* **2011**, *23*, 3134−3138.
(17) Korte, K. E.; Skrabalak, S. E.; Xia, Y. Rapid Synthesis of Silver Nanowires through a CuCl- or CuCl2-Mediated Polyol Process. *J. Mater. Chem.* **2008**, *18*, 437.
(18) Pacholski, C.; Kornowski, A.; Weller, H. Self-Assembly of ZnO: From Nanodots to Nanorods. *Angew. Chem., Int. Ed.* **2002**, *41*, 1188−1191.
(19) Khaligh, H. H.; Goldthorpe, I. A. Failure of Silver Nanowire Transparent Electrodes under Current Flow. *Nanoscale Res. Lett.* **2013**, *8*, 2−6.
(20) Nelson, J. *The Physics of Solar Cells*, 1 ed.; Imperial College Press: London, 2003; p 384.
(21) Kang, H. S.; Du Ahn, B.; Kim, J. H.; Kim, G. H.; Lim, S. H.; Chang, H. W.; Lee, S. Y. Structural, Electrical, and Optical Properties of P-Type ZnO Thin Films with Ag Dopant. *Appl. Phys. Lett.* **2006**, *88*, 202108.
(22) Schmidt, M.; Masson, a.; Bréchignac, C. Oxygen and Silver Clusters: Transition from Chemisorption to Oxidation. *Phys. Rev. Lett.* **2003**, *91*, 243401.
(23) Tvarusko, A. The Electric Resistivity of AgO. *J. Electrochem. Soc.* **1968**, *115*, 1105−1110.
(24) Willis, S. M.; Cheng, C.; Assender, H. E.; Watt, A. A. R. The Transitional Heterojunction Behavior of PbS/ZnO Colloidal Quantum Dot Solar Cells. *Nano Lett.* **2012**, *12*, 1522−1526.

DOI: 10.1021/am505646d
ACS Appl. Mater. Interfaces 2015, 7, 6417−6421